ADVANCED ENERGY MATERIALS
www.advenergymat.de

Side-Chain Engineering on Y-Series Acceptors with Chlorinated End Groups Enables High-Performance Organic Solar Cells

Yuzhong Chen, Ruijie Ma, Tao Liu, Yiqun Xiao, Ha Kyung Kim, Jianquan Zhang,* Chao Ma, Huiliang Sun, Fujin Bai, Xugang Guo, Kam Sing Wong, Xinhui Lu,* and He Yan**

Chemical modifications of non-fullerene acceptors (NFAs) play vital roles in the development of high efficiency organic solar cells (OSCs). In this work, on the basis of the previously reported molecule named Y6-1O, chlorination and inner side-chain engineering are adopted to endow the corresponding devices with higher open-circuit voltage (V_{OC}) and short-circuit current density (J_{SC}) as well as good morphology for high fill factor (FF). As a result, the molecule named BTP1O-4Cl-C12 can help achieve a higher power conversion efficiency (PCE) of 17.1% than that of Y6-1O (16.1%). Furthermore, the following comparisons between BTP1O-4Cl-C12 and the two symmetric acceptors named BTP2O-4Cl-C12 and BTP-4Cl-C12 demonstrate the effect of asymmetric alkoxy substitution on the outer side chains, which not only achieves a balance between V_{OC} and J_{SC}, but also help obtain appropriate morphology for efficient charge dissociation and suppressed charge recombination. Therefore, the asymmetric BTP1O-4Cl-C12 can achieve a higher PCE compared to the symmetric BTP2O-4Cl-C12 and BTP-4Cl-C12. The work not only reports an excellent NFA for high-performance OSCs, but also puts forward a series of methods for consecutive chemical modifications on Y-series acceptors, which can be further applied to boost the PCE of OSCs to a higher level.

1. Introduction

Organic solar cells (OSCs) have attracted great attention in the past decade due to their several attractive features such as light weight, flexibility, portability, low-cost, and large-scale applications.[1–8] During the development of the materials used for OSCs, non-fullerene acceptors (NFAs) play vital roles to push the device efficiencies to a high level.[9–19] Among them, the emerging Y-series acceptors exhibit excellent optoelectronic properties and contribute to excellent photovoltaic performances of over 17%.[20–29] Therefore, it is important to understand the structure-property relationships of Y-series acceptors and figure out effective methods to further optimize their chemical structures.

Typically, Y-series acceptors consist of three parts: the electron-deficient core with the rigid aromatic systems, the electron-withdrawing end groups and two sets

Dr. Y. Chen, R. Ma, Dr. T. Liu, H. K. Kim, Dr. J. Zhang, F. Bai, Prof. H. Yan
Department of Chemistry
Guangdong-Hong Kong-Macao Joint Laboratory of Optoelectronic and Magnetic Functional Materials
Energy Institute and Hong Kong Branch of Chinese National Engineering Research Center for Tissue Restoration & Reconstruction
Hong Kong University of Science and Technology
Clear Water Bay, Kowloon, Hong Kong SAR, P. R. China
E-mail: liutaozhx@ust.hk; jzhangbn@connect.ust.hk; hyan@ust.hk

Dr. Y. Chen, R. Ma, Dr. T. Liu, H. K. Kim, Dr. J. Zhang, F. Bai, Prof. H. Yan
HKUST-Shenzhen Research Institute
No. 9 Yuexing 1st Road, Hi-tech Park, Nanshan, Shenzhen 518057, P. R. China

Y. Xiao, Prof. X. Lu
Department of Physics
Chinese University of Hong Kong
New Territories, Hong Kong 999077, P. R. China
E-mail: xinhui.lu@cuhk.edu.hk

The ORCID identification number(s) for the author(s) of this article can be found under https://doi.org/10.1002/aenm.202003777.

Dr. C. Ma, Prof. K. S. Wong
Department of Physics
Hong Kong University of Science and Technology
Clear Water Bay, Kowloon, Hong Kong SAR, P. R. China

Dr. H. Sun, Prof. X. Guo
Department of Materials Science and Engineering and The Shenzhen Key Laboratory for Printed Organic Electronics Southern University of Science and Technology (SUSTech)
Xueyuan Road, Shenzhen, Guangdong 518055, P. R. China

Prof. H. Yan
Institute of Polymer Optoelectronic Materials and Devices
State Key Laboratory of Luminescent Materials and Devices
South China University of Technology (SCUT)
Guangzhou 510640, P. R. China

DOI: 10.1002/aenm.202003777

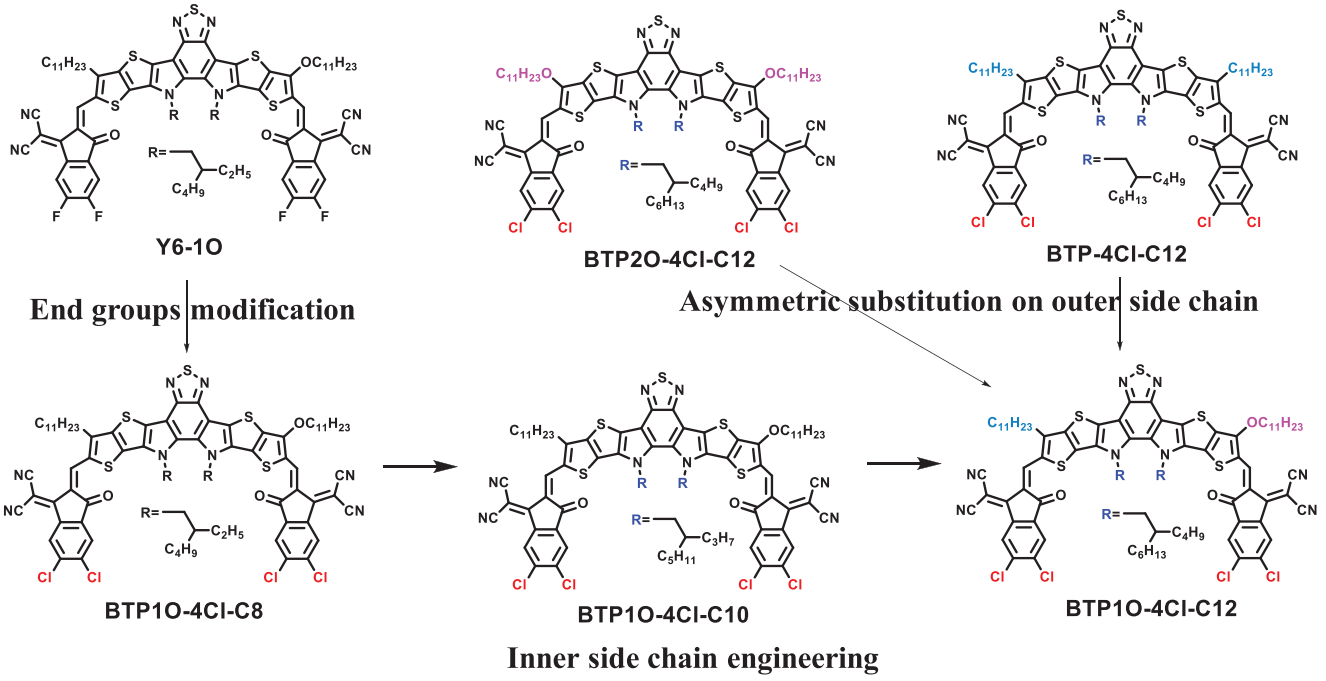

Figure 1. Chemical structure of Y6-1O, BTP1O-4Cl-C8, BTP1O-4Cl-C10, BTP1O-4Cl-C12, BTP2O-4Cl-C12, and BTP-4Cl-C12.

of side chains (in the inner and outer positions) with the configuration of A-DA'D-A.[30–32] All the three parts can be reasonably designed and regulated to fine-tune the molecular properties of Y-series acceptors.[33–41] For example, if the chlorine atoms are used to replace the fluorine atoms in one of the famous Y-series acceptors named Y6,[42] the resulting molecule BTP-4Cl not only exhibits red-shifted absorption but also reduced voltage loss, leading to the BTP-4Cl-based devices showing an increased power conversion efficiency (PCE) of 16.5% with enhanced open-circuit voltage (V_{OC}) and short-circuit current density (J_{SC}) compared to those of the Y6-based devices.[43] It is also promising to modify the inner branched side chains which determine the solubility and crystallinity of Y-series acceptors. By replacing the 2-ethylhexyl chains of Y6 with the longer 2-butyloctyl ones, the enhancement in solubility and electron mobility of the resulting molecule named BTP-4F-12 not only yielded a higher PCE of 16.4% but also enabled device processing by environmentally friendly solvents.[44]

Besides the progress in the aforementioned chemical modifications of Y-series acceptors, the outer side chains on the β-positions of the thienothiophene units also have several key effects. First of all, the outer side chains can render the molecules with sufficient solubility.[45] Besides, the outer side-chain engineering can also change the optoelectronic properties of the molecules with variant energy levels and absorption ranges.[46] Last but not least, the outer side chains can introduce steric hindrance between the rigid fused cores and the end groups, resulting in the so-called "conformational locking effect" to reduce the number of stereoisomers and change the planarity of the molecules, which will in turn affect the molecular packing and change the morphological properties of the active layers.[47–49] Previously, our group have devoted a lot of efforts in outer side-chain engineering,[19,46,50,51] among which the asymmetric alkyl-alkoxy substitution strategy has shown great potential for the Y-series acceptors since this modification can maintain the advantages of alkoxy substitution to achieve a higher V_{OC} while preventing over-aggregation caused by the alkoxy groups. As a result, the asymmetric acceptor named Y6-1O (**Figure 1**)-based ternary devices can achieve an excellent PCE of 17.6%.[50]

Despite the high performance using ternary strategy, binary devices based on Y6-1O only showed a moderate PCE of 16.1%, which can be further improved through rational chemical modification. Therefore, in this work, we first replaced the fluorine atoms of the end groups in Y6-1O with the chlorine atoms to obtain a new acceptor named BTP1O-4Cl-C8. Although the BTP1O-4Cl-C8-based device exhibited a slightly higher V_{OC} and J_{SC}, the excessive aggregation property caused by the replacement from F to Cl delivered a much lower fill factor (FF) of 69.9% and thus an inferior PCE of 14.7%. To solve this problem, inner side-chain engineering was taken to extend the 2-ethylhexyl chains of BTP1O-4Cl-C8 to the 2-propylheptyl (BTP1O-4Cl-C10) and 2-butyloctyl ones (BTP1O-4Cl-C12). BTP1O-4Cl-C10 still showed relatively poor solubility in chloroform at room temperature but can be dissolved well upon heating. Therefore, hot-solvent processing was adopted to fabricate the BTP1O-4Cl-C10-based devices, generating a higher FF of 77.6% and PCE of 16.4%. Furthermore, BTP1O-4Cl-C12 has even better solubility that the corresponding devices can be directly processed at room temperature, achieving the highest FF of 78.8% and PCE of 17.1%. Finally, we compared the optoelectronic properties and photovoltaic performance of BTP1O-4Cl-C12 with two symmetric acceptors named BTP2O-4Cl-C12 and BTP-4Cl-C12. It is found that BTP1O-4Cl-C12-based devices can obtain a good balance between V_{OC} and J_{SC} while achieving the highest FF and thus the best performance, which again proves the wide applications of our asymmetric alkyl-alkoxy substitution strategy in Y-series acceptors.

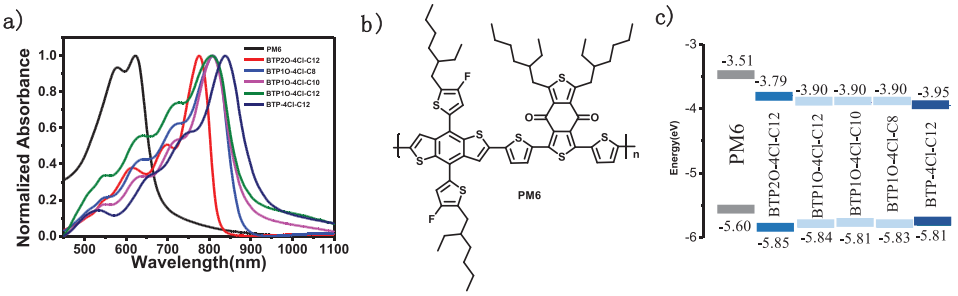

Figure 2. a) Normalized absorption spectra of PM6, BTP1O-4Cl-C8, BTP1O-4Cl-C10, BTP1O-4Cl-C12, BTP2O-4Cl-C12, and BTP-4Cl-C12 in pristine films; b) The chemical structure of PM6; c) The energy levels alignment of PM6, BTP1O-4Cl-C8, BTP1O-4Cl-C10, BTP1O-4Cl-C12, BTP2O-4Cl-C12, and BTP-4Cl-C12.

2. Results and Discussion

The chemical structure of BTP1O-4Cl-C8, BTP1O-4Cl-C10, BTP1O-4Cl-C12, BTP2O-4Cl-C12 and BTP-4Cl-C12, and their design strategy are summarized in Figure 1. First we replaced the fluorine atoms of the end groups in Y6-1O with chlorine atoms to obtain BTP1O-4Cl-C8. Through inner side-chain engineering, BTP1O-4Cl-C10 and BTP1O-4Cl-C12 were synthesized by replacing 2-ehylhexyl with 2-propylheptyl and 2-butyloctyl, respectively. In addition, the symmetric BTP2O-4Cl-C12 and BTP-4Cl-C12 were designed for comparisons.[33] All the molecules can be synthesized through Knoevenagel condensations between the corresponding dialdehyde precursors and the dichloro-substituted end groups as shown in Scheme S1 (Supporting Information). The detailed synthesis procedures are described in the Supporting Information with the corresponding NMR and mass spectra of the final small molecules. BTP1O-4Cl-C8 and BTP1O-4Cl-C10 cannot dissolve well in chloroform at room temperature but show relatively better solubility in hot chloroform, while the other three molecules can dissolve well in chloroform at room temperature. According to the thermogravimetric analysis results (TGA) shown in Figure S1a (Supporting Information), the decomposition temperature (T_d, 5% weight loss) of all five molecules are above 280 °C, which shows their great thermal stability for the applications in OSC devices. To further investigate the difference of the molecular aggregation and crystallinity, differential scanning calorimetry (DSC) measurement was taken as shown in Figure S1b (Supporting Information). BTP1O-4Cl-C8 decomposed before melting so that its melting temperature (T_m) and enthalpy change (ΔH_m) remain unknown. Compared to the T_m of 306 °C with a ΔH_m of 23.7 J g^{-1} for BTP1O-4Cl-C10, BTP1O-4Cl-C12 shows a lower T_m of 302 °C but a greater ΔH_m of 30.3 J g^{-1}, which indicates the extension of inner side chains from 2-propylheptyl to 2-butyloctyl can achieve better molecular packing and crystallinity. Besides, BTP2O-4Cl-C12 has the highest T_m with the highest ΔH_m of 66.1 J g^{-1} due to the strong intermolecular interaction and high crystallinity caused by the symmetric alkoxy substitution. The T_m and ΔH_m of BTP1O-4Cl-C12 are slightly higher than those of BTP-4Cl-C12 (290 °C and 28.5 J g^{-1}), which confirms that the asymmetric alkoxy substitution can cause slight enhancement in crystallinity of the molecules but prevent their over-aggregation.

The ultraviolet–visible (UV–vis) measurements were carried out to obtain the absorption spectra of the five acceptors in dilute chloroform solutions and thin films, shown in Figure S2a (Supporting Information) and **Figure 2a**, respectively (the corresponding parameters are listed in **Table 1**). All the five molecules show obvious redshifts and vibration shoulder peaks arising in the absorption spectra of the neat films compared to those in solution, indicating the strong molecular packing in the solid state. BTP1O-4Cl-C8, BTP1O-4Cl-C10, and BTP1O-4Cl-C12 are found to have almost same absorption range in chloroform. They also exhibit similar absorption spectra in neat films, implying few changes in optical bandgaps are caused by the extension of the branched alkyl chains. But a small difference exists in the low-energy area that the absorption tails gradually appear from BTP1O-4Cl-C8, BTP1O-4Cl-C10 to BTP1O-4Cl-C12, which is due to the decrease in molecular aggregation.[45] Same as our previous work, alkoxy side chains cause obvious

Table 1. Summary of optical and electronic parameters for BTP1O-4Cl-C8, BTP1O-4Cl-C10, BTP1O-4Cl-C12, BTP2O-4Cl-C12, and BTP-4Cl-C12.

Acceptor	λ_{max}[a)] [nm]	λ_{max}[b)] [nm]	λ_{onset}[a)] [nm]	λ_{onset}[b)] [nm]	$E_g^{optc)}$ [eV]	HOMO[d)] [eV]	LUMO[d)] [eV]	$E_g^{elee)}$ [eV]
BTP1O-4Cl-C8	730	809	777	869	1.43	−5.83	−3.90	1.93
BTP1O-4Cl-C10	729	808	777	882	1.41	−5.81	−3.90	1.91
BTP1O-4Cl-C12	729	806	777	878	1.41	−5.84	−3.90	1.94
BTP2O-4Cl-C12	714	776	750	818	1.52	−5.85	−3.79	2.06
BTP-4Cl-C12	745	838	798	918	1.35	−5.81	−3.95	1.86

[a)]In solution state (Chloroform); [b)]In pure films; [c)]Obtained with equation: $E_g^{opt} = 1240/\lambda_{onset}$[b)]; [d)]Measured by cyclic voltammetry (CV) method; [e)]Obtained with equation: E_g^{ele} = LUMO-HOMO.

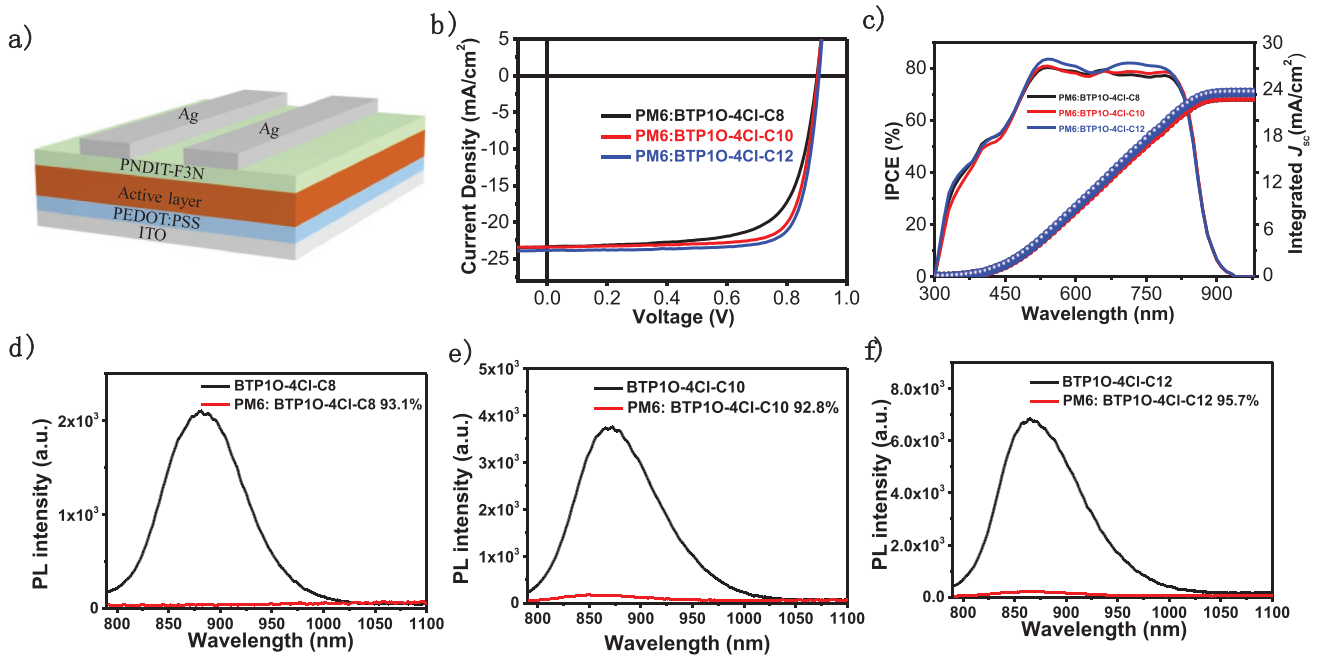

Figure 3. a) Device structure; b) Current density-voltage (*J-V*) curves of OSCs based on PM6:BTP1O-4Cl-C8, PM6:BTP1O-4Cl-C10, and PM6:BTP1O-4Cl-C12; c) Corresponding EQE spectra of PM6:BTP1O-4Cl-C8, PM6:BTP1O-4Cl-C10, and PM6:BTP1O-4Cl-C12-based devices; Photoluminescence spectra of d) BTP1O-4Cl-C8, e) BTP1O-4Cl-C10, and f) BTP1O-4Cl-C12-based films excited at 785 nm.

blue-shifted spectra from BTP-4Cl-C12, BTP1O-4Cl-C12 to BTP2O-4Cl-C12 with the increased optical bandgap from 1.35, 1.41 to 1.52 eV, respectively.[50] According to Figure 2a, the absorption ranges of all five acceptors are complementary to that of the medium-bandgap polymer PM6 (structure shown in Figure 2b), which has strong absorption in the range of 400–700 nm and can work well with most of Y-series acceptors.

To further investigate the energy levels of these five acceptors, cyclic voltammetry (CV) measurements were performed by using Ag/Ag^+ as the reference and Fc/Fc^+ (–4.80 eV) redox couple as the external standard. The CV plots of the films based on these five acceptors are shown in Figure S3 (Supporting Information), and the corresponding results are summarized in Table 1. According to energy level alignment shown in Figure 2c, the HOMO and LUMO levels of BTP1O-4Cl-C8, BTP1O-4Cl-C10, and BTP1O-4Cl-C12 are almost the same, indicating the extension of inner side chains has negligible effects on energy levels so that the absorption spectra are also similar. The alkoxy substitutions on the outer side chains, however, can significantly change the electrochemical properties of Y-series acceptors by upshifting the LUMO levels while maintaining the HOMO levels, which results in widening bandgaps. Since the LUMO levels increase gradually from BTP-4Cl-C12 to BTP1O-4Cl-C12 and to BTP2O-4Cl-C12, it is expected that the alkoxy substitutions afford higher V_{OC} for the corresponding devices.

To understand the impact of the chlorinated end groups and inner side-chain modification, we first fabricated OSC devices based on BTP1O-4Cl-C8, BTP1O-4Cl-C10, and BTP1O-4Cl-C12 with the conventional device structure as shown in **Figure 3a**, i.e., (ITO)/poly(3,4-ethylenedioxythiophene): poly (styrene sulfonate) (PEDOT:PSS)/PM6:NFAs/Poly[[2,7-bis(2-ethylhexyl)-1,2,3,6,7,8-hexahydro-1,3,6,8-tetraoxobenzo[lmn][3,8]phenanthroline-4,9-diyl]-2,5-thiophenediyl[9,9-bis[3-(dimethylamino)propyl]-9H-fluorene-2,7-diyl]-2,5-thiophenediyl] (PNDIT-F3N) /Ag. Considering the poor solubility of BTP1O-4Cl-C8 and BTP1O-4Cl-C10 in chloroform at room temperature, hot-solvent processing was used to spin-cast the active layers. But for BTP1O-4Cl-C12, with good solubility at room temperature in chloroform, no heating condition was needed, which simplified the device fabrication process. The detailed device fabrication conditions are summarized in the Supporting Information. The optimal photovoltaic parameters of the devices based on these three acceptors are summarized in **Table 2** with the corresponding *J–V* curves depicted in Figure 3b.

Compared to the photovoltaic parameters of the Y6-1O-based devices, the chlorinated BTP1O-4Cl-C8-based devices

Table 2. The photovoltaic parameters of OSCs based on BTP1O-4Cl-C8, BTP1O-4Cl-C10, BTP1O-4Cl-C12.

Active layer	V_{OC} [V]	J_{SC} [mA cm^{-2}][a)]	FF [%]	PCE [%][b)]
PM6:BTP1O-4Cl-C8	0.90	23.37 (22.97)	69.9	14.7 (14.4)
PM6:BTP1O-4Cl-C10	0.90	23.42 (23.00)	77.6	16.4 (16.1)
PM6:BTP1O-4Cl-C12	0.91	23.85 (23.55)	78.8	17.1 (16.7)
PM6:Y6-1O[c)]	0.89	23.2 (23.0)	78.3	16.1 (15.4)
PM6:BTP2O-4Cl-C12	0.96	21.14 (21.09)	77.2	15.6 (15.3)
PM6:BTP-4Cl-C12	0.85	25.73 (25.07)	74.6	16.3 (16.1)

[a)]The values in bracket are obtained by integration of the EQE curves; [b)]The values in bracket are the average PCE of 20 devices; [c)]Data from the literature.[50]

can achieve a slightly higher V_{OC} and J_{SC}, which agrees well with the previously reported literature.[43] But the FF dramatically decreases from 78.3% to 69.9%, which indicates the poor morphology of the blend films possibly due to the excessive aggregation property and poor solubility of BTP1O-4Cl-C8. Therefore, the device performance of BTP1O-4Cl-C8 (14.7%) is even worse than that of Y6-1O. The extension of the inner side chains can address the morphology issue to obtain excellent FF. As shown in Table 2, in addition to the slight enhancement in V_{OC} and J_{SC}, the FF of the devices based on BTP1O-4Cl-C8, BTP1O-4Cl-C10, and BTP1O-4Cl-C12 increases from 69.9% to 77.6% and to 78.8%. As a result, an outstanding PCE of 17.1% can be achieved by the BTP1O-4Cl-C12-based OSCs with a V_{OC} of 0.91 V, a J_{SC} of 23.85 mA cm^{-2}, and a FF of 78.8%. Although the BTP1O-4Cl-C10-based devices can also achieve a moderate PCE of 16.4%, the high cost of the intermediates, 3-(bromomethyl)heptane, and the hot-solvent processing make it not the ideal material for OSCs compared to BTP1O-4Cl-C12. To test the reproducibility of these OSCs, twenty devices of each acceptor were made to calculate the mean values and standard deviations of photovoltaic parameters as listed in Table S1 (Supporting Information).

The external quantum efficiency (EQE) spectra of the devices based on BTP1O-4Cl-C8, BTP1O-4Cl-C10, and BTP1O-4Cl-C12 were acquired (Figure 3c). All the three devices exhibit a broad and high photon response from 300 to 900 nm, which are consistent with the absorption of the corresponding blend films (Figure S2b, Supporting Information). The integrated J_{SC} of the three devices from the EQE spectra also agrees well with the values measured from the J–V curves (Table 2). It is very clear that the BTP1O-4Cl-C12-based device has the highest EQE values in the range of 500–800 nm among the three devices, indicating the most efficient photon-to-electron conversion in the PM6:BTP1O-4Cl-C12 blend. As a result, the BTP1O-4Cl-C12-based devices can achieve a higher J_{SC} compared to the BTP1O-4Cl-C8 and BTP1O-4Cl-C10-based ones.

Time-resolved photoluminescence (TRPL) technique is used to further understand the differences in J_{SC} caused by the charge generation process of the three blends. As shown in Figure S4a (Supporting Information), although BTP1O-4Cl-C8, BTP1O-4Cl-C10, and BTP1O-4Cl-C12-based blends show similar photoluminescence decay process, the decay dynamics of the neat BTP1O-4Cl-C12 film is the slowest, which indicates the longest exciton lifetime of BTP1O-4Cl-C12. Therefore, PM6:BTP1O-4Cl-C12 blend film should exhibit more efficient exciton dissociation for charge transfer.[52,53] Besides, steady-state photoluminescence (PL) measurements were taken to figure out the efficiency of the exciton dissociation. As shown in Figure 3d–f, the quenching efficiency of the PM6:BTP1O-4Cl-C12 film (95.7%) is higher than that of PM6:BTP1O-4Cl-C8 (93.1%) and PM6:BTP1O-4Cl-C10 blend ones (92.8%), demonstrating more efficient exciton dissociation, hole transfer and the highest EQE and J_{SC} of this material combination.[41]

In order to probe the charge mobility of the three blends, the space-charge-limited current (SCLC) methods were employed (Figure S5a,b: Supporting Information) to calculate the hole and electron mobility (μ_h and μ_e). As summarized in Table S2 (Supporting Information), both μ_h and μ_e increase from PM6:BTP1O-4Cl-C8 (5.81×10^{-4} and 3.05×10^{-4} cm^2 V^{-1} s^{-1}), PM6:BTP1O-4Cl-C10 (6.10×10^{-4} and 3.57×10^{-4} cm^2 V^{-1} s^{-1}) to PM6:BTP1O-4Cl-C12 (6.28×10^{-4} and 3.81×10^{-4} cm^2 V^{-1} s^{-1}). In addition, the PM6:BTP1O-4Cl-C12 blend also shows a more balanced charge transport with a smaller μ_h/μ_e ratio of 1.65 than those of PM6:BTP1O-4Cl-C8 (1.90) and PM6:BTP1O-4Cl-C10 (1.71). The high and balanced charge mobility contributes to the high FF for the OSCs based on PM6:BTP1O-4Cl-C12.[54,55]

To estimate the interaction between donor and acceptor that are relevant to nanoscale phase separation from the perspective of molecular interactions, the contact angle measurements were performed to study the surface tension (γ) of PM6, BTP1O-4Cl-C8, BTP1O-4Cl-C10, and BTP1O-4Cl-C12. The contact angle images of the four films using water and ethylene glycol (EG) as the solvents are provided in Figure S6a–d (Supporting Information). By Fowkes method, the γ values of the materials are calculated from measured contact angles on water and EG (Table S3, Supporting Information).[56,57] As a result, the γ for PM6, BTP1O-4Cl-C8, BTP1O-4Cl-C10, and BTP1O-4Cl-C12 are determined to be 32.1, 58.3, 27.2, and 23.2 mN m^{-1}, respectively, which shows that BTP1O-4Cl-C10 and BTP1O-4Cl-C12 have similar γ while BTP1O-4Cl-C8 has a dramatically higher γ. Accordingly, the interaction parameters (χ) between each pair of material combinations were acquired through the Flory-Huggins model (Table S3, Supporting Information). The results show that the interaction parameter between PM6 and BTP1O-4Cl-C8 is the highest (χ = 3.901), indicating low miscibility between these two materials.[58,59] This should be due to its excessive aggregation property, which causes the poor morphology of the blend films and a low FF of the corresponding devices.[60,61] In contrast, both PM6:BTP1O-4Cl-C10 and PM6:BTP1O-4Cl-C12 show small χ values (0.203 and 0.710, respectively), which implies remarkable miscibility between PM6 and these two acceptors towards good morphology and high FF.[62]

Next, we investigated the effects of the asymmetric alkyl-alkoxy substitution strategy in BTP1O-4Cl-C12 by comparing the device performance of BTP2O-4Cl-C12, BTP1O-4Cl-C12, and BTP-4Cl-C12. First, density-functional theory (DFT) calculations were carried out at B3LYP/6-31G* level to calculate the optimized molecular geometries and frontier molecular orbitals (FMOs) of BTP2O-4Cl-C12, BTP1O-4Cl-C12, and BTP-4Cl-C12. Since the length of alkyl chains have little effects on energy levels and molecular geometry, the long side chains were simplified with methyl, ethyl or methoxy groups to shorten the calculation time. As shown in Table S4 (Supporting Information), all the three molecules show similar molecular geometry, indicating few changes caused by the alkoxy substitution. But the alkoxy groups upshift the calculated LUMO levels of BTP-4Cl, BTP1O-4Cl, and BTP2O-4Cl from −3.62, −3.57 to −3.46 eV while their HOMO levels are similar (≈−5.60) eV, which is also supported by CV measurements. Furthermore, the dipole moments of BTP-4Cl, BTP1O-4Cl, and BTP2O-4Cl increase from 1.18, 3.45 to 4.96 D, which implies the gradually enhanced intermolecular interactions.[63,64] The increase of dipole moments can be explained by the corresponding electronic potential diagram shown in Table S4 (Supporting Information), where the alkoxy groups push the electrons from the core to the end groups. Also, alkoxy substitutions can bring stronger intramolecular

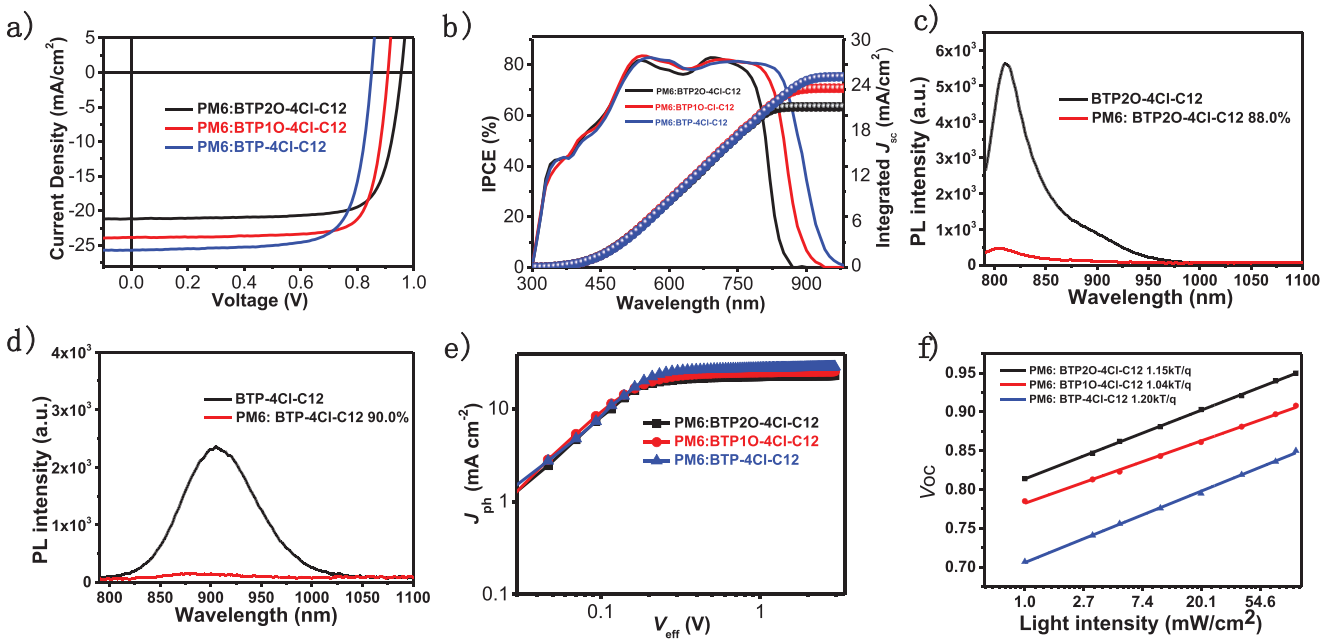

Figure 4. a) Current density–voltage (*J–V*) curves of OSCs based on PM6:BTP2O-4Cl-C12, PM6:BTP1O-4Cl-C12, and PM6:BTP-4Cl-C12; b) Corresponding EQE spectra of PM6:BTP2O-4Cl-C12, PM6:BTP1O-4Cl-C12, and PM6:BTP-4Cl-C12-based devices; Photoluminescence spectra of c) BTP2O-4Cl-C12 and d) BTP-4Cl-C12-based films excited at 785 nm; e) J_{ph} versus V_{eff} of the optimized devices based on BTP2O-4Cl-C12, BTP1O-4Cl-C12, and BTP-4Cl-C12; f) V_{OC} of the optimized devices based on BTP2O-4Cl-C12, BTP1O-4Cl-C12, and BTP-4Cl-C12 versus light intensity.

conformational locking effect than alkyl substitutions, which can also enhance the packing of the molecules.[50]

To further support the calculation results, the molecular packing of BTP2O-4Cl-C12, BTP1O-4Cl-C12, and BTP-4Cl-C12 were studied by the 2D grazing incidence wide-angle X-ray scattering (GIWAXS). The 2D GIWAXS patterns and the corresponding 10° sector averaged 2D-GIWAXS profiles of three neat films are shown in Figure S7 (Supporting Information) with the morphological data summarized in Table S4 (Supporting Information).[65] All the three films exhibit strong (010) peak in the out-of-plane direction, indicating their preferential face-on orientation. The (010) diffraction peaks of BTP2O-4Cl-C12, BTP1O-4Cl-C12, and BTP-4Cl-C12 are located at 1.73, 1.73, and 1.76 Å^{-1}, which stands for the d-spacing of 3.63, 3.63, and 3.57 Å, respectively. It should be noted that the coherence lengths (CLs) of the (010) peaks of BTP2O-4Cl-C12, BTP1O-4Cl-C12, and BTP-4Cl-C12 calculated by Scherrer equation are 20.1, 18.7, and 17.0 Å, which indicates the decreased molecular packing. Besides, in the in-plane direction, both BTP1O-4Cl-C12 and BTP-4Cl-C12 only show one peak at 0.38 Å^{-1} with the d-spacing of 16.5 Å. But for BTP2O-4Cl-C12, there are two peaks at 0.39 and 0.26 Å^{-1} respectively, demonstrating more ordered structures with the d-spacing of 24.1 and 16.1 Å. The 2D-GIWAXS results as well as calculation results support that alkoxy substitutions can enhance the molecular packing of the molecules, which can change the blend morphology and the charge transport properties.

In order to investigate the photovoltaic performance of BTP2O-4Cl-C12, BTP1O-4Cl-C12, and BTP-4Cl-C12, the conventional OSCs were fabricated with the same device structure shown in Figure 3a. Still, PM6 was chosen as the donor polymer and the detailed fabrication conditions are summarized in the Supporting Information. The *J–V* curves are shown in **Figure 4a**, and the photovoltaic parameters of the optimized devices are collected in Table 2. It is obvious from the *J–V* curves that the V_{OC} the devices increases from BTP-4Cl-C12 (0.85 V), BTP1O-4Cl-C12 (0.91 V) to BTP2O-4Cl-C12 (0.96 V), which is consistent with the higher LUMO levels measured by CV and DFT calculation results. Meanwhile, the J_{SC} decreases form BTP-4Cl-C12 (25.73 mA cm^{-2}), BTP1O-4Cl-C12 (23.85 mA cm^{-2}) to BTP2O-4Cl-C12 (21.14 mA cm^{-2}) caused by the blue-shifted absorption onset. It should be noted that the energy loss (E_{loss}, equal to the difference between E_g and qV_{OC}, in which E_g is the optical bandgap of donor or acceptor whichever has a smaller value) of the BTP2O-4Cl-C12-based devices (0.56 eV) is much higher than those of BTP-4Cl-C12 and BTP1O-4Cl-C12-based devices (0.50 and 0.50 eV), which limits its potential to achieve higher PCEs. And the PM6:BTP1O-4Cl-C12-based devices can also achieve the highest FF of 78.8% among the three acceptors, which contributes to the higher PCE of 17.1% than those of the BTP2O-4Cl-C12 and BTP-4Cl-C12-based devices (15.6% and 16.3%).

Further EQE measurements were taken to figure out the reason for the different J_{SC} of the three devices. According to the EQE spectra in Figure 4b, all the three devices can maintain similar and high EQE values of over 70% in their absorption range (Figure S2b, Supporting Information) and the integrated J_{SC} of BTP2O-4Cl-C12 and BTP-4Cl-C12-based devices are also consistent with the measured J_{SC} within an error of 3% (Table 2). The EQE spectra clearly support that the decrease of J_{SC} from BTP-4Cl-C12, BTP1O-4Cl-C12 to BTP2O-4Cl-C12 is mainly because of the blue-shifted absorption onset since the alkoxy substitution upshifts the LUMO levels without largely affecting the HOMO levels.

Table 3. Morphology data of BTP2O-4Cl-C12, BTP1O-4Cl-C12, BTP-4Cl-C12 blend films.

Samples	In plane			Out of plane		
	location [Å^{-1}]	*d*-spacing[a)] [Å]	CL[b)] [Å]	location [Å^{-1}]	*d*-spacing[a)] [Å]	CL[b)] [Å]
PM6:BTP2O-4Cl-C12	0.29	21.6	53.7	0.34	18.5	70.3
	0.44	14.3	57.4	0.43	14.6	82.6
	0.63	9.97	32.4	1.74	3.61	28.1
PM6:BTP1O-4Cl-C12	0.29	21.6	66.2	1.75	3.59	23.4
PM6:BTP-4Cl-C12	0.29	21.6	77.3	1.73	3.61	21.7

[a)]Obtained by the equation of $d = 2\pi/q$, in which q is the corresponding x-coordinate of diffraction peak; [b)]Calculated using the equation: CL = $2\pi K$/w, in which w is the full width at half maxima and K is a form factor (0.9 here).

Then, blend morphology was investigated since it can significantly affect the device performance. First, the contact angle measurements were further performed to study the surface tension of BTP2O-4Cl-C12 and BTP-4Cl-C12. The contact angle images of the two neat films using water and EG as solvent are provided in Figure S6e,f (Supporting Information) with corresponding γ and χ listed in Table S3 (Supporting Information). All the pure films of BTP-4Cl-C12, BTP1O-4Cl-C12, and BTP2O-4Cl-C12 show similar γ (28.4, 23.2, and 24.9 mN m^{-1}) and close to that of PM6 (32.1 mN m^{-1}), which cause small χ of each pair of PM6 and three acceptors (0.11, 0.71, and 0.45), indicating the miscibility of donor and acceptor is not the determining factor for the differences of FF. Next, atomic force microscopy (AFM) was utilized to probe the surface morphology of the blend films based on BTP2O-4Cl-C12, BTP1O-4Cl-C12, and BTP-4Cl-C12. Figure S8 (Supporting Information) provides the corresponding AFM height sensor images and phase images. All the PM6: BTP-4Cl-C12, PM6:BTP1O-4Cl-C12, and PM6: BTP2O-4Cl-C12 blends show small root-mean-square (RMS) roughness (0.71, 0.75, and 1.20 nm), which indicate their smooth surface for efficient charge transport from the photoactive layer to the charge transporting layer.

Furthermore, 2D GIWAXS was performed to better understand the effects of alkoxy substitution on blend film morphology. As the 2D patterns shown in Figure S7d (Supporting Information) and morphology data listed in Table S5 (Supporting Information), the neat PM6 film shows a strong (100) peak in the in-plane direction at 0.30 Å^{-1} and a (010) peak in the out-of-plane direction at 1.72 Å^{-1}. The 2D patterns of the PM6:BTP2O-4Cl-C12, PM6:BTP1O-4Cl-C12, and PM6:BTP-4Cl-C12 blends and the corresponding GIWAXS profiles are displayed in **Figure 5**a–d. Compared to the 2D pattern of the pure PM6 film, after blending with three acceptors, all the 2D patterns of the three blends show predominant (010) peak in the out-of-plane direction coming from three NFAs and PM6, which indicates all three blend films form face-on orientation that is beneficial for vertical charge transport.[66] Similar to the neat films, the CLs of the (010) peak increase from PM6:BTP-4Cl-C12 (21.7 Å), PM6:BTP1O-4Cl-C12 (23.4 Å) to PM6:BTP2O-4Cl-C12 (28.1 Å) blend (**Table 3**). Besides, the BTP2O-4Cl-C12-based blend also shows high-ordered peaks in the out of plane direction with low q-values of 0.34 and 0.43 Å^{-1} and very large CLs of 70.3 and 82.6 Å, proving the good molecular packing of BTP2O-4Cl-C12 due to the alkoxy substitution. In conclusion of these morphology characterizations, although PM6 has good miscibility with all the three acceptors, the enhanced aggregation property caused by alkoxy groups increase the molecular packing from PM6:BTP-4Cl-C12, PM6:BTP1O-4Cl-C12 to PM6:BTP2O-4Cl-C12, which should be beneficial for charge mobility of the corresponding devices.

By the SCLC method (Figure S5, Supporting Information), μ_h and μ_e of the BTP2O-4Cl-C12, BTP1O-4Cl-C12, and BTP-4Cl-C12-based devices were measured to study the effect of the alkoxy substitution on charge mobility. As listed in Table S2 (Supporting Information), both devices of PM6:BTP1O-4Cl-C12 and PM6:BTP-4Cl-C12 show higher μ_h and μ_e ($6.28 \times 10^{-4}/3.81 \times 10^{-4}$ and $7.11 \times 10^{-4}/3.85 \times 10^{-4}$ cm^2 V^{-1} s^{-1}, respectively) than those of the PM6:BTP2O-4Cl-C12-based one ($5.39 \times 10^{-4}/3.17 \times 10^{-4}$ cm^2 V^{-1} s^{-1}). Besides, the μ_h/μ_e ratios of the BTP2O-4Cl-C12, BTP1O-4Cl-C12, and BTP-4Cl-C12-based blend are calculated to be 1.70, 1.65 and 1.85, respectively. The higher charge mobility and more balanced charge transport contribute to the highest FF of the PM6:BTP1O-4Cl-C12-based OSCs.[54,55]

TRPL technique was taken again to analyze the dynamics and efficiency of the charge generation process. As shown in Figure S4b (Supporting Information), for the neat films, BTP1O-4Cl-C12 shows the slowest decay which indicates its longest exciton lifetime. Since the photoluminescence decay process of three blend films is similar, it is supposed that more efficient exciton dissociation happens in BTP1O-4Cl-C12 blends.[52,53] To further support this observation, steady-state PL quenching experiment was employed to calculate the quenching efficiency of BTP2O-4Cl-C12 and BTP-4Cl-C12 blends. According to the PL spectra shown in Figures 3f and 4c,d, the PM6:BTP1O-4Cl-C12-based film has the highest PL quenching efficiency of 95.7% while those of PM6:BTP2O-4Cl-C12 and PM6:BTP-4Cl-C12-based films are 88.0% and 90.0%, respectively, demonstrating that PM6:BTP1O-4Cl-C12-based film shows the most efficient hole transfer.[46]

The charge generation and collection efficiency of the three OSCs are investigated by measuring the photocurrent density (J_{ph}) versus effective voltage (V_{eff}), wherein J_{ph} is defined as $J_{ph} = J_L - J_D$ and V_{eff} is determined as $V_{eff} = V_0 - V_{bias}$. Here, J_L and J_D are photocurrent densities under standard illumination condition and in the dark condition, respectively, while V_0 is the voltage when J_{ph} is zero and V_{bias} is the external voltage bias.[67] The value of V_{eff} will affect the electric field in the devices and change the exciton dissociation and collection process. According to Figure 4e, the J_{ph} when V_{eff} = 3.0 V was chosen as the saturated current density (J_{sat}). The exciton dissociation

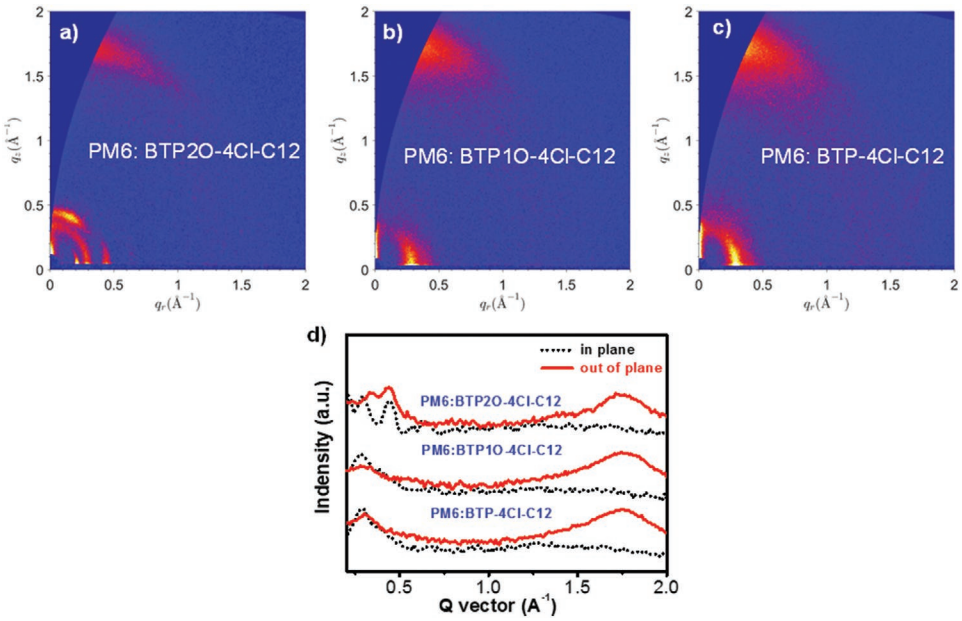

Figure 5. 2D-GIWAXS patterns: a) a PM6:BTP2O-4Cl-C12 blend film; b) a PM6:BTP1O-4Cl-C12 blend film; c) a PM6:BTP-4Cl-C12 blend film; d) In-plane (blank) and out-of-plane (red) line cuts of the corresponding 2D-GIWAXS patterns for BTP2O-4Cl-C12, BTP1O-4Cl-C12, BTP-4Cl-C12 blend films.

probability (P_{diss}) and charge collection efficiency (P_{coll}) of the devices can be characterized by the ratio between J_{ph} and J_{sat} under short-circuit condition and maximum power output, respectively.[68] The P_{diss} and P_{coll} of OSCs based on BTP2O-4Cl-C12, BTP1O-4Cl-C12, and BTP-4Cl-C12 were calculated and summarized in Table S6 (Supporting Information). The P_{diss} and P_{coll} values of the BTP1O-4Cl-C12-based devices are 94.0% and 84.6%, respectively, which are higher than those of the BTP2O-4Cl-C12-based (92.9% and 82.4%) and BTP-4Cl-C12-based ones (90.9% and 80.4%). These results indicate that the BTP1O-4Cl-C12-based OSCs have more efficient charge dissociation and collection compared to those based on the other two acceptors, which contributes to the higher J_{SC} and FF.[69]

The charge recombination process of the three OSCs were studied by measuring the dependence of J_{SC} and V_{OC} on different light intensity (P_{light}). At short-circuit condition, the J_{SC} should be proportional to $P_{light}{}^{\alpha}$, where α stands for the degree of bimolecular recombination.[70] The ideal α is equal to 1 while the experimental α is always smaller than 1 due to some extent of bimolecular recombination.[71] As shown in Figure S8 (Supporting Information), the α values of the OSCs based on BTP2O-4Cl-C12, BTP1O-4Cl-C12, and BTP-4Cl-C12 are 0.948, 0.966, and 0.934, respectively. The slightly higher α value of the BTP1O-4Cl-C12-based devices indicates lower bimolecular recombination. Besides, the V_{OC} and P_{light} should follow the formula of $V_{OC} \propto n(KT/q)\ln(P)$, where n, q, T, and K are the ideality factor, the elementary charge, temperature (K) and Boltzmann constant, respectively.[72] The value of n indicates the degree of trap-assisted recombination. n equal to 2 means trap-assisted recombination dominates in the devices while n closer to 1 means less trap-assisted recombination.[73] According to Figure 4f, the n values of the BTP2O-4Cl-C12, BTP1O-4Cl-C12, and BTP-4Cl-C12-based devices are 1.16, 1.05 and 1.20, respectively, which implies significantly lower trap-assisted recombination of BTP1O-4Cl-C12-based devices. Overall, the BTP1O-4Cl-C12-based devices suffer from the least charge recombination, which accounts for the high FF.

3. Conclusion

In summary, on the basis of the previous reported Y-series acceptor named Y6-1O, we first replaced the end groups with the chlorinated ones. Despite the slightly higher V_{OC} and J_{SC}, the dramatically decreased FF of devices based on BTP1O-4Cl-C8 limits the final OSC performance. Therefore, extending inner side-chain engineering was taken to obtain two new NFAs named BTP1O-4Cl-C10 and BTP1O-4Cl-C12. Among them, BTP1O-4Cl-C12 has the best solubility that can be processed at room temperature. The devices based on BTP1O-4Cl-C12 can obtain the highest FF of 78.8% as well as maintain the higher V_{OC} and J_{SC}, which help achieve an excellent PCE of 17.1% that outperforms Y6-1O. The following investigations on the effects of alkoxy groups by choosing two symmetric NFAs named BTP2O-4Cl-C12 and BTP-4Cl-C12 as comparisons again demonstrate the advantages of asymmetric alkoxy substitution on the outer side chains. BTP1O-4Cl-C12 can not only make a balance between J_{SC} and V_{OC} to achieve low energy loss but help achieve high FF by high and balanced charge mobility and suppressed charge recombination. This work applies a series of strategies to modify a Y-series acceptor, which can also be used in other Y-series acceptors to further improve the photovoltaic performance of OSCs.

Supporting Information

Supporting Information is available from the Wiley Online Library or from the author.

Acknowledgements

Y.C. and R.M. contributed equally to this work. The work described in this paper was partially supported by the National Key Research and Development Program of China (No. 2019YFA0705900) funded by MOST, the Basic and Applied Basic Research Major Program of Guangdong Province (No. 2019B030302007), Guangdong-Hong Kong-Macao Joint Laboratory of Optoelectronic and Magnetic Functional Materials (project number 2019B121205002), the Shen Zhen Technology and Innovation Commission (project number JCYJ20170413173814007, JCYJ20170818113905024), the Hong Kong Research Grants Council (Research Impact Fund R6021-18, collaborative research fund C6023-19G, project numbers 16309218, 16310019, and 16303917), Hong Kong Innovation and Technology Commission for the support through projects ITC-CNERC14SC01 and ITS/471/18), National Natural Science Foundation of China (NSFC, No. 91433202).

Conflict of Interest

The authors declare no conflict of interest.

Data Availability Statement

Research data are not shared.

Keywords

chlorinated end groups, organic solar cells, side-chain engineering, Y-series acceptors

Received: December 6, 2020
Revised: February 23, 2021
Published online:

[1] L. Schmidt-Mende, A. Fechtenkötter, K. Müllen, E. Moons, R. H. Friend, J. D. MacKenzie, *Science* **2001**, *293*, 1119.
[2] P. Cheng, X. Zhan, *Chem. Soc. Rev.* **2016**, *45*, 2544.
[3] D. Baran, R. S. Ashraf, D. A. Hanifi, M. Abdelsamie, N. Gasparini, J. A. Röhr, S. Holliday, A. Wadsworth, S. Lockett, M. Neophytou, C. J. M. Emmott, J. Nelson, C. J. Brabec, A. Amassian, A. Salleo, T. Kirchartz, J. R. Durrant, I. McCulloch, *Nat. Mater.* **2017**, *16*, 363.
[4] S.-Y. Chang, P. Cheng, G. Li, Y. Yang, *Joule* **2018**, *2*, 1039.
[5] J. Zhang, H. S. Tan, X. Guo, A. Facchetti, H. Yan, *Nat. Energy* **2018**, *3*, 720.
[6] H. Sun, X. Guo, A. Facchetti, *Chem* **2020**, *6*, 1310.
[7] A. Wadsworth, M. Moser, A. Marks, M. S. Little, N. Gasparini, C. J. Brabec, D. Baran, I. McCulloch, *Chem. Soc. Rev.* **2019**, *48*, 1596.
[8] Y. Tong, Z. Xiao, X. Du, C. Zuo, Y. Li, M. Lv, Y. Yuan, C. Yi, F. Hao, Y. Hua, T. Lei, Q. Lin, K. Sun, D. Zhao, C. Duan, X. Shao, W. Li, H.-L. Yip, Z. Xiao, B. Zhang, Q. Bian, Y. Cheng, S. Liu, M. Cheng, Z. Jin, S. Yang, L. Ding, *Sci. China: Chem.* **2020**, *63*, 758.
[9] P. Cheng, G. Li, X. Zhan, Y. Yang, *Nat. Photonics* **2018**, *12*, 131.
[10] C. Yan, S. Barlow, Z. Wang, H. Yan, A. K. Y. Jen, S. R. Marder, X. Zhan, *Nat. Rev. Mater.* **2018**, *3*, 18003.
[11] G. Zhang, J. Zhao, P. C. Y. Chow, K. Jiang, J. Zhang, Z. Zhu, J. Zhang, F. Huang, H. Yan, *Chem. Rev.* **2018**, *118*, 3447.
[12] J. Hou, O. Inganäs, R. H. Friend, F. Gao, *Nat. Mater.* **2018**, *17*, 119.
[13] L. Meng, Y. Zhang, X. Wan, C. Li, X. Zhang, Y. Wang, X. Ke, Z. Xiao, L. Ding, R. Xia, H.-L. Yip, Y. Cao, Y. Chen, *Science* **2018**, *361*, 1094.
[14] Y. Chen, T. Liu, H. Hu, T. Ma, J. Y. L. Lai, J. Zhang, H. Ade, H. Yan, *Adv. Energy Mater.* **2018**, *8*, 1801203.
[15] T. Liu, W. Gao, G. Zhang, L. Zhang, J. Xin, W. Ma, C. Yang, H. Yan, C. Zhan, J. Yao, *Sol. RRL* **2019**, *3*, 1800376.
[16] T. Liu, W. Gao, Y. Wang, T. Yang, R. Ma, G. Zhang, C. Zhong, W. Ma, H. Yan, C. Yang, *Adv. Funct. Mater.* **2019**, *29*, 1902155.
[17] T. Liu, R. Ma, Z. Luo, Y. Guo, G. Zhang, Y. Xiao, T. Yang, Y. Chen, G. Li, Y. Yi, X. Lu, H. Yan, B. Tang, *Energy Environ. Sci.* **2020**, *13*, 2115.
[18] L. Zhu, M. Zhang, G. Zhou, T. Hao, J. Xu, J. Wang, C. Qiu, N. Prine, J. Ali, W. Feng, X. Gu, Z. Ma, Z. Tang, H. Zhu, L. Ying, Y. Zhang, F. Liu, *Adv. Energy Mater.* **2020**, *10*, 1904234.
[19] R. Ma, Y. Tao, Y. Chen, T. Liu, Z. Luo, Y. Guo, Y. Xiao, J. Fang, G. Zhang, X. Li, X. Guo, Y. Yi, M. Zhang, X. Lu, Y. Li, H. Yan, *Sci. China: Chem.* **2021**, https://doi.org/10.1007/s11426-020-9912-0.
[20] R. Ma, T. Liu, Z. Luo, K. Gao, K. Chen, G. Zhang, W. Gao, Y. Xiao, T.-K. Lau, Q. Fan, Y. Chen, L.-K. Ma, H. Sun, G. Cai, T. Yang, X. Lu, E. Wang, C. Yang, A. K. Y. Jen, H. Yan, *ACS Energy Lett.* **2020**, *5*, 2711.
[21] L. Liu, Y. Kan, K. Gao, J. Wang, M. Zhao, H. Chen, C. Zhao, T. Jiu, A.-K. Y. Jen, Y. Li, *Adv. Mater.* **2020**, *32*, 1907604.
[22] Z. Luo, R. Ma, T. Liu, J. Yu, Y. Xiao, R. Sun, G. Xie, J. Yuan, Y. Chen, K. Chen, G. Chai, H. Sun, J. Min, J. Zhang, Y. Zou, C. Yang, X. Lu, F. Gao, H. Yan, *Joule* **2020**, *4*, 1236.
[23] Y. Lin, M. I. Nugraha, Y. Firdaus, A. D. Scaccabarozzi, F. Aniés, A.-H. Emwas, E. Yengel, X. Zheng, J. Liu, W. Wahyudi, E. Yarali, H. Faber, O. M. Bakr, L. Tsetseris, M. Heeney, T. D. Anthopoulos, *ACS Energy Lett.* **2020**, *5*, 3663.
[24] H. Fu, W. Gao, Y. Li, F. Lin, X. Wu, J. H. Son, J. Luo, H. Y. Woo, Z. Zhu, A. K. Y. Jen, *Small Methods* **2020**, *4*, 2000687.
[25] L. Arunagiri, Z. Peng, X. Zou, H. Yu, G. Zhang, Z. Wang, J. Y. Lin Lai, J. Zhang, Y. Zheng, C. Cui, F. Huang, Y. Zou, K. S. Wong, P. C. Y. Chow, H. Ade, H. Yan, *Joule* **2020**, *4*, 1790.
[26] D. Li, L. Zhu, X. Liu, W. Xiao, J. Yang, R. Ma, L. Ding, F. Liu, C. Duan, M. Fahlman, Q. Bao, *Adv. Mater.* **2020**, *32*, 2002344.
[27] Y. Lin, B. Adilbekova, Y. Firdaus, E. Yengel, H. Faber, M. Sajjad, X. Zheng, E. Yarali, A. Seitkhan, O. M. Bakr, A. El-Labban, U. Schwingenschlögl, V. Tung, I. McCulloch, F. Laquai, T. D. Anthopoulos, *Adv. Mater.* **2019**, *31*, 1902965.
[28] L. Zhan, S. Li, T.-K. Lau, Y. Cui, X. Lu, M. Shi, C.-Z. Li, H. Li, J. Hou, H. Chen, *Energy Environ. Sci.* **2020**, *13*, 635.
[29] R. Ma, T. Liu, Z. Luo, Q. Guo, Y. Xiao, Y. Chen, X. Li, S. Luo, X. Lu, M. Zhang, Y. Li, H. Yan, *Sci. China: Chem.* **2020**, *63*, 325.
[30] J. Yuan, H. Zhang, R. Zhang, Y. Wang, J. Hou, M. Leclerc, X. Zhan, F. Huang, F. Gao, Y. Zou, Y. Li, *Chem* **2020**, *6*, 2147.
[31] J. Zhao, C. Yao, M. U. Ali, J. Miao, H. Meng, *Mater. Chem. Front.* **2020**, *4*, 3487.
[32] S. Li, C.-Z. Li, M. Shi, H. Chen, *ACS Energy Lett.* **2020**, *5*, 1554.
[33] Y. Cui, H. Yao, L. Hong, T. Zhang, Y. Tang, B. Lin, K. Xian, B. Gao, C. An, P. Bi, W. Ma, J. Hou, *Natl. Sci. Rev.* **2019**, *7*, 1239.
[34] K. Jiang, Q. Wei, J. Y. L. Lai, Z. Peng, H. K. Kim, J. Yuan, L. Ye, H. Ade, Y. Zou, H. Yan, *Joule* **2019**, *3*, 3020.
[35] T. Liu, Y. Zhang, Y. Shao, R. Ma, Z. Luo, Y. Xiao, T. Yang, X. Lu, Z. Yuan, H. Yan, Y. Chen, Y. Li, *Adv. Funct. Mater.* **2020**, *30*, 2000456.
[36] Z. Zhou, W. Liu, G. Zhou, M. Zhang, D. Qian, J. Zhang, S. Chen, S. Xu, C. Yang, F. Gao, H. Zhu, F. Liu, X. Zhu, *Adv. Mater.* **2020**, *32*, 1906324.
[37] S. Dong, T. Jia, K. Zhang, J. Jing, F. Huang, *Joule* **2020**, *4*, 2004.
[38] Z. Luo, R. Ma, Z. Chen, Y. Xiao, G. Zhang, T. Liu, R. Sun, Q. Zhan, Y. Zou, C. Zhong, Y. Chen, H. Sun, G. Chai, K. Chen, X. Guo, J. Min, X. Lu, C. Yang, H. Yan, *Adv. Energy Mater.* **2020**, *10*, 2002649.
[39] S. Liu, J. Yuan, W. Deng, M. Luo, Y. Xie, Q. Liang, Y. Zou, Z. He, H. Wu, Y. Cao, *Nat. Photonics* **2020**, *14*, 300.
[40] C. Sun, S. Qin, R. Wang, S. Chen, F. Pan, B. Qiu, Z. Shang, L. Meng, C. Zhang, M. Xiao, C. Yang, Y. Li, *J. Am. Chem. Soc.* **2020**, *142*, 1465.

[41] G. Chai, J. Zhang, M. Pan, Z. Wang, J. Yu, J. Liang, H. Yu, Y. Chen, A. Shang, X. Liu, F. Bai, R. Ma, Y. Chang, S. Luo, A. Zeng, H. Zhou, K. Chen, F. Gao, H. Ade, H. Yan, *ACS Energy Lett.* **2020**, *5*, 3415.
[42] J. Yuan, Y. Zhang, L. Zhou, G. Zhang, H.-L. Yip, T.-K. Lau, X. Lu, C. Zhu, H. Peng, P. A. Johnson, M. Leclerc, Y. Cao, J. Ulanski, Y. Li, Y. Zou, *Joule* **2019**, *3*, 1140.
[43] Y. Cui, H. Yao, J. Zhang, T. Zhang, Y. Wang, L. Hong, K. Xian, B. Xu, S. Zhang, J. Peng, Z. Wei, F. Gao, J. Hou, *Nat. Commun.* **2019**, *10*, 2515.
[44] L. Hong, H. Yao, Z. Wu, Y. Cui, T. Zhang, Y. Xu, R. Yu, Q. Liao, B. Gao, K. Xian, H. Y. Woo, Z. Ge, J. Hou, *Adv. Mater.* **2019**, *31*, 1903441.
[45] Y. Cui, H. Yao, J. Zhang, K. Xian, T. Zhang, L. Hong, Y. Wang, Y. Xu, K. Ma, C. An, C. He, Z. Wei, F. Gao, J. Hou, *Adv. Mater.* **2020**, *32*, 1908205.
[46] G. Chai, Y. Chang, Z. Peng, Y. Jia, X. Zou, D. Yu, H. Yu, Y. Chen, P. C. Y. Chow, K. S. Wong, J. Zhang, H. Ade, L. Yang, C. Zhan, *Nano Energy* **2020**, *76*, 105087.
[47] J. Wu, J. Lee, Y.-C. Chin, H. Yao, H. Cha, J. Luke, J. Hou, J.-S. Kim, J. R. Durrant, *Energy Environ. Sci.* **2020**, *13*, 2422.
[48] C. Zhang, J. Yuan, K. L. Chiu, H. Yin, W. Liu, G. Zheng, J. K. W. Ho, S. Huang, G. Yu, F. Gao, Y. Zou, S. K. So, *J. Mater. Chem. A* **2020**, *8*, 8566.
[49] Q. Wei, W. Liu, M. Leclerc, J. Yuan, H. Chen, Y. Zou, *Sci. China: Chem.* **2020**, *63*, 1352.
[50] Y. Chen, F. Bai, Z. Peng, L. Zhu, J. Zhang, X. Zou, Y. Qin, H. K. Kim, J. Yuan, L.-K. Ma, J. Zhang, H. Yu, P. C. Y. Chow, F. Huang, Y. Zou, H. Ade, F. Liu, H. Yan, *Adv. Energy Mater.* **2021**, *11*, 2003141.
[51] X. Ma, A. Zeng, J. Gao, Z. Hu, C. Xu, J. H. Son, S. Y. Jeong, C. Zhang, M. Li, K. Wang, H. Yan, Z. Ma, Y. Wang, H. Y. Woo, F. Zhang, *Natl. Sci. Rev.* **2020**, https://doi.org/10.1093/nsr/nwaa305.
[52] Z. Liu, N. Wang, *Adv. Opt. Mater.* **2019**, *7*, 1900913.
[53] A. Classen, C. L. Chochos, L. Lüer, V. G. Gregoriou, J. Wortmann, A. Osvet, K. Forberich, I. McCulloch, T. Heumüller, C. J. Brabec, *Nat. Energy* **2020**, *5*, 711.
[54] W. Li, S. Albrecht, L. Yang, S. Roland, J. R. Tumbleston, T. McAfee, L. Yan, M. A. Kelly, H. Ade, D. Neher, W. You, *J. Am. Chem. Soc.* **2014**, *136*, 15566.
[55] C. M. Proctor, J. A. Love, T.-Q. Nguyen, *Adv. Mater.* **2014**, *26*, 5957.
[56] K.-H. Kim, H. Kang, H. J. Kim, P. S. Kim, S. C. Yoon, B. J. Kim, *Chem. Mater.* **2012**, *24*, 2373.
[57] S. Nilsson, A. Bernasik, A. Budkowski, E. Moons, *Macromolecules* **2007**, *40*, 8291.
[58] L. Ye, W. Zhao, S. Li, S. Mukherjee, J. H. Carpenter, O. Awartani, X. Jiao, J. Hou, H. Ade, *Adv. Energy Mater.* **2017**, *7*, 1602000.
[59] L. Ye, H. Hu, M. Ghasemi, T. Wang, B. A. Collins, J.-H. Kim, K. Jiang, J. H. Carpenter, H. Li, Z. Li, T. McAfee, J. Zhao, X. Chen, J. L. Y. Lai, T. Ma, J.-L. Bredas, H. Yan, H. Ade, *Nat. Mater.* **2018**, *17*, 253.
[60] Z. Zhang, L. Yang, Z. Hu, J. Yu, X. Liu, H. Wang, J. Cao, F. Zhang, W. Tang, *Mater. Chem. Front.* **2020**, *4*, 1747.
[61] C. Yang, S. Zhang, J. Ren, M. Gao, P. Bi, L. Ye, J. Hou, *Energy Environ. Sci.* **2020**, *13*, 2864.
[62] R. Ma, G. Li, D. Li, T. Liu, Z. Luo, G. Zhang, M. Zhang, Z. Wang, S. Luo, T. Yang, F. Liu, H. Yan, B. Tang, *Sol. RRL* **2020**, *4*, 2000250.
[63] M. Li, Y. Zhou, J. Zhang, J. Song, Z. Bo, *J. Mater. Chem. A* **2019**, *7*, 8889.
[64] C. Li, H. Fu, T. Xia, Y. Sun, *Adv. Energy Mater.* **2019**, *9*, 1900999.
[65] A. Hexemer, W. Bras, J. Glossinger, E. Schaible, E. Gann, R. Kirian, A. MacDowell, M. Church, B. Rude, H. Padmore, *J. Phys.: Conf. Ser.* **2010**, *247*, 012007.
[66] P. Müller-Buschbaum, *Adv. Mater.* **2014**, *26*, 7692.
[67] P. W. M. Blom, V. D. Mihailetchi, L. J. A. Koster, D. E. Markov, *Adv. Mater.* **2007**, *19*, 1551.
[68] Z. He, C. Zhong, X. Huang, W.-Y. Wong, H. Wu, L. Chen, S. Su, Y. Cao, *Adv. Mater.* **2011**, *23*, 4636.
[69] N. Gasparini, M. Salvador, S. Strohm, T. Heumueller, I. Levchuk, A. Wadsworth, J. H. Bannock, J. C. de Mello, H.-J. Egelhaaf, D. Baran, I. McCulloch, C. J. Brabec, *Adv. Energy Mater.* **2017**, *7*, 1700770.
[70] Y. Zang, C.-Z. Li, C.-C. Chueh, S. T. Williams, W. Jiang, Z.-H. Wang, J.-S. Yu, A. K. Y. Jen, *Adv. Mater.* **2014**, *26*, 5708.
[71] I. Riedel, J. Parisi, V. Dyakonov, L. Lutsen, D. Vanderzande, J. C. Hummelen, *Adv. Funct. Mater.* **2004**, *14*, 38.
[72] W. L. Leong, S. R. Cowan, A. J. Heeger, *Adv. Energy Mater.* **2011**, *1*, 517.
[73] M. M. Mandoc, F. B. Kooistra, J. C. Hummelen, B. de Boer, P. W. M. Blom, *Appl. Phys. Lett.* **2007**, *91*, 263505.